

8. Patthey, F. *et al.* High-resolution photoemission study of the low-energy excitations in 4f-electron systems. *Phys. Rev. B* **42**, 8864–8881 (1990).
9. Weschke, E. *et al.* Surface and bulk electronic structure of Ce metal studied by high-resolution resonant photoemission. *Phys. Rev. B* **44**, 8304–8307 (1991).
10. Kaindl, G. *et al.* Status and perspectives of high-resolution spectroscopy in the soft x-ray range. *Rev. Sci. Instrum.* **63**, 1234–1240 (1992).
11. Joyce, J. J. *et al.* Temperature-invariant photoelectron spectra in cerium heavy-fermion compounds: Inconsistencies with the Kondo model. *Phys. Rev. Lett.* **68**, 236–239 (1992).
12. Duò, L. *et al.* The Ce 4f surface shift: A test for the Anderson-impurity Hamiltonian. *Phys. Rev. B* **54**, R17363–R17366 (1996).
13. Garnier, M. *et al.* Applicability of the single impurity model to photoemission spectroscopy of heavy fermion Ce compounds. *Phys. Rev. Lett.* **78**, 4127–4130 (1997).
14. Amato, A. *et al.* Thermopower and magneto-thermopower of CeRu₂Si₂ single crystals. *J. Magn. Magn. Mater.* **76 & 77**, 263–264 (1988).
15. Aoki, H., Uji, S., Albessard, A. K. & Ônuki, Y. Observation of heavy electrons in CeRu₂Si₂ via the dHvA effect. *J. Phys. Soc. Jpn* **61**, 3457–3461 (1992).
16. Hedo, M. *et al.* Magnetoresistance and de Haas-van Alphen oscillation in normal and superconducting CeRu₂. *Phil. Mag. B* **77**, 975–1000 (1998).
17. Yang, S.-H. *et al.* High-resolution photoemission study of CeRu₂: The dual character of 4f electrons. *Phys. Rev. B* **53**, R11946–R11948 (1996).
18. Kang, J.-S. *et al.* Photoemission study of an f-electron superconductor: CeRu₂. *Phys. Rev. B* **60**, 5348–5353 (1999).
19. Gunnarsson, O. & Schönhammer, K. Photoemission from Ce compounds: Exact model calculation in the limit of large degeneracy. *Phys. Rev. Lett.* **50**, 604–607 (1983).
20. Allen, J. W. *et al.* Electronic structure of cerium and light rare-earth intermetallics. *Adv. Phys.* **35**, 275–316 (1986).
21. Bickers, N. E., Cox, D. L. & Wilkins, J. W. Thermodynamic, transport and excitation properties of Ce impurities in a model metal: Kondo resonance and universality in the mixed-valent regime. *Phys. Rev. Lett.* **54**, 230–233 (1985).
22. Yeh, J. J. & Lindau, I. Atomic subshell photoionization cross sections and asymmetry parameters $1 \leq Z \leq 103$. *At. Data Nucl. Data Tables* **32**, 1–155 (1985).
23. Witkowski, N. *et al.* Resonant photoemission study of the 4f spectral function of cerium in Ce/Fe(100) interfaces. *Phys. Rev. B* **56**, 12054–12057 (1997).

Acknowledgements

We thank S. Ueda, M. Kotsugi, K. Kadono and R.-J. Jung, and the staffs of SPring-8 and PF, especially T. Matsushita, T. Nakatani, T. Muro, K. Mamiya and A. Kakizaki. We also thank S. Imada for discussions. This work was supported by a Grant-in-Aid for COE Research from the Ministry of Education, Science, Sports and Culture of Japan. The work was performed under the approvals of the PF PAC and of the Japan Synchrotron Radiation Research Institute.

Correspondence and requests for materials should be addressed to A.S. (e-mail: sekizama@mp.es.osaka-u.ac.jp).

Dynamic instabilities and memory effects in vortex matter

Y. Paltiel*, E. Zeldov*†, Y. N. Myasoedov*, H. Shtrikman*, S. Bhattacharya‡§, M. J. Higgins‡, Z. L. Xiao||, E. Y. Andreii||, P. L. Gammel† & D. J. Bishop†

* Department of Condensed Matter Physics, The Weizmann Institute of Science, Rehovot 76100, Israel

† Bell Laboratories, Lucent Technologies, Murray Hill, New Jersey 07974, USA

‡ NEC Research Institute, 4 Independence Way, Princeton, New Jersey 08540, USA

§ Tata Institute of Fundamental Research, Mumbai-400005, India

|| Department of Physics and Astronomy, Rutgers University, Piscataway, New Jersey 08855, USA

The magnetic flux line lattice in type II superconductors serves as a useful system in which to study condensed matter flow, as its dynamic properties are tunable. Recent studies have shown a number of puzzling phenomena associated with vortex motion, including: low-frequency noise^{1–5} and slow voltage oscillations^{3,6}; a history-dependent dynamic response^{7–12}, and memory of the direction, amplitude duration and frequency of the previously applied current^{13,14}; high vortex mobility for alternating current, but no apparent vortex motion for direct currents^{13,15,16}; and strong suppression of an a.c. response by small d.c. bias¹³. Taken

together, these phenomena are incompatible with current understanding of vortex dynamics. Here we report a generic mechanism that accounts for these observations. Our model, which is derived from investigations of the current distribution across single crystals of NbSe₂, is based on a competition between the injection of a disordered vortex phase at the sample edges, and the dynamic annealing of this metastable disorder by the transport current. For an alternating current, only narrow regions near the edges are in the disordered phase, while for d.c. bias, most of the sample is in the disordered phase—preventing vortex motion because of more efficient pinning. The resulting spatial dependence of the disordered vortex system serves as an active memory of the previous history.

In conventional superconductors like NbSe₂, the anomalous phenomena are found^{1,2,7–11,13–15} in the vicinity of the ‘peak effect’ where the critical current I_c increases sharply below the upper critical field H_{c2} (Fig. 1a). The peak effect marks a structural transformation^{1,2,7–11,17} of the vortex lattice: below the peak region an ordered phase (OP) is present, which is dominated by the elastic energy of the lattice and is, therefore, weakly pinned. On approaching the peak region, however, the increased softening of the lattice causes a transition into a disordered vortex phase (DP), which accommodates better to the pinning landscape, resulting in a sharp increase in I_c . In high-temperature superconductors like Bi₂Sr₂Ca-Cu₂O₈, this situation is equivalent to the second magnetization peak¹⁸, where the ordered Bragg-glass phase is believed to transform into a disordered solid^{19–21}. Figure 1a shows the I_c measured at various frequencies. On the high-temperature side of the peak effect, I_c is frequency independent; in this region the disordered vortex phase is thermodynamically stable. In contrast, on the low-temperature side, a significant frequency dependence is observed^{13,15}; in this region, all the unusual vortex response phenomena appear^{1,2,7–11,13–15}. As described below, a dynamic coexistence of the ordered vortex phase and a metastable disordered vortex phase is established in this region in the presence of an applied current. We first outline the proposed mechanism, and then present the experimental evidence.

The first ingredient of the proposed model is the observation that in NbSe₂ the disordered vortex phase can be readily supercooled to below the peak effect by field cooling, where it remains metastable, as the thermal fluctuations are negligible^{8–11}. This supercooled disordered phase is pinned more strongly and displays a significantly larger critical current density (J_c^{dis}) than that of the stable ordered phase (J_c^{ord}). An externally applied current in excess of J_c^{dis} serves as an effective temperature and ‘anneals’ the metastable disordered vortex phase, as observed by transport⁸, magnetic response¹⁰, decoration²², and small-angle neutron scattering (SANS) experiments²³ on NbSe₂.

The second ingredient of the model is the presence of substantial surface barriers²⁴, as observed recently²⁵ in NbSe₂. Consider a steady-state flow of an ordered vortex phase in the presence of a transport current. In the standard platelet strip geometry, in a perpendicular field B , vortices penetrate from one edge of the sample and leave at the opposite edge. In the absence of a surface barrier, vortex penetration does not require any extra force. As a result, the vortices penetrate close to their proper vortex lattice locations, as dictated by the elastic forces of the lattice. In the presence of a surface barrier, however, a large force is required for vortex penetration and exit, and hence much of the applied current flows at the edges in order to provide the necessary driving force^{25–28}. The surface barrier is known to be very sensitive to surface imperfections. Therefore, the penetrating vortices are injected predominantly at the weakest points of the barrier, thus destroying the local order and forming a metastable disordered vortex phase near the edge, which drifts into the sample with the flow of the entire lattice. (Note that steps on the surface or extended defects in inhomogeneous samples could also act as injection points of the

disordered phase). The applied current, therefore, has two effects: the current that flows at the edges causes ‘contamination’ by injecting a disordered vortex phase, while the current that flows in the bulk acts as an annealing mechanism. The observed dynamic instabilities and memory phenomena arise for the fine balance between these two competing processes.

The annealing process is sensitive to the exact location on the $H - T$ phase diagram. Below the peak effect, the disordered vortex phase is highly unstable and therefore its relaxation time τ_r in the presence of a driving force is very short. As a result, it anneals rapidly over a characteristic ‘healing’ length $L_r = v\tau_r$, where v is the vortex lattice drift velocity. The corresponding profile of the local critical

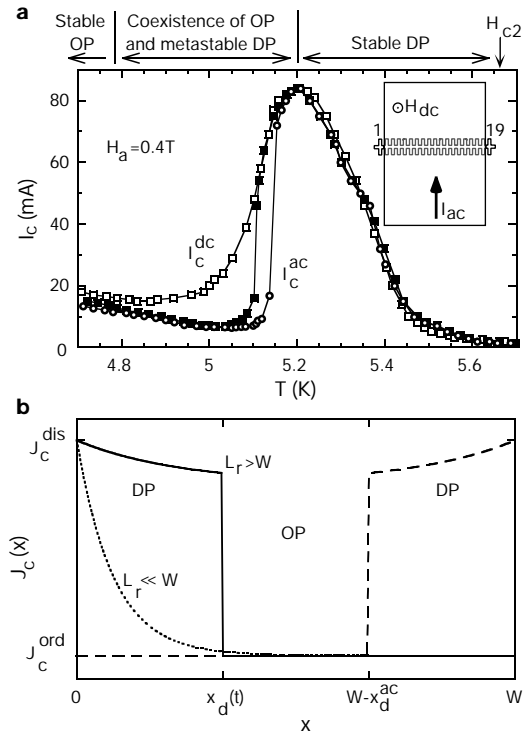


Figure 1 Critical current versus temperature, and the dynamic coexistence of the ordered and disordered phases. **a**, The peak effect in critical current I_c in NbSe₂ crystal A versus temperature, as measured with a d.c. drive, I_c^{dc} (open squares), and a.c. drive, I_c^{ac} , at 181 (filled squares) and 881 Hz (circles). The critical current was determined resistively using a voltage criterion of 1 μ V. At low temperatures only the stable ordered vortex phase (OP) is present. On the lower-temperature side of the peak effect, a metastable disordered vortex phase (DP) coexists dynamically with the stable ordered phase, resulting in a frequency-dependent I_c . On the high-temperature side of the peak effect, only the stable disordered phase is present with no anomalous behaviour. Inset, experimental set-up. Several Fe-doped (200 p.p.m.) single crystals of 2H-NbSe₂ were investigated. Here we report data on crystal A of $2.6 \times 0.34 \times 0.05$ mm³ and $T_c = 6.0$ K, and crystal B of $2.4 \times 0.29 \times 0.02$ mm³ with $T_c = 6.05$ K. Four electrical contacts were attached to the top surface for transport measurements, with the voltage contact separation of 0.6 ± 0.2 mm. The surface of the crystal was attached to an array of 19 two-dimensional electron gas (2DEG) Hall sensors 10×10 μ m² each. The vortex lattice was initially prepared in the ordered phase by zero-field-cooling to a low temperature at which the disordered phase is unstable, and then slowly heated to the desired temperature in the presence of a constant field H_a applied parallel to the c axis. **b**, Schematic plot of the local critical current density $J_c(x)$ across a crystal of width W . J_c^{dis} and J_c^{ord} are the values of the critical current density in the fully disordered phase and in the ordered phase, respectively. For $L_r \ll W$ the disordered phase relaxes rapidly into ordered phase resulting in the dotted $J_c(x)$ in the steady-state d.c. flow. For $L_r > W$, the disordered phase penetrates to a depth $x_d(t)$ following the application of direct current at $t = 0$ (solid curve). For an alternating current at $t = T_{ac}/2$, the disordered phase occupies the left edge to a depth of x_d^{ac} (solid curve), and symmetrically the right edge at $t = T_{ac}$ (dashed curve).

current density $J_c(x)$ should therefore decay from J_c^{dis} to J_c^{ord} over the characteristic length scale L_r , as illustrated by the dotted line in Fig. 1b. Note that L_r and τ_r are generally current dependent, and decrease dramatically at elevated currents⁸. On the other hand, near the peak effect the free energies of the disordered and the ordered phases are comparable, and therefore the ‘life-times’ of the disordered phase τ_r and the corresponding L_r are very large. As a result, the front of the disordered phase, given by $x_d(t)$, progressively penetrates into the bulk as shown by the solid line in Fig. 1b, until the entire sample is contaminated. In this situation the experimental, steady-state d.c. critical current I_c^{dc} does not reflect an equilibrium property, but rather a dynamic coexistence of two phases. It is given by $I_c^{dc} = d \int_0^W J_c(x) dx \approx dL_r J_c^{dis} + d(W - L_r) J_c^{ord}$ for $L_r < W$, and $I_c^{dc} \approx I_c^{dis} = dW J_c^{dis}$ for $L_r \gg W$, where d and W are the thickness and width of the sample, respectively (neglecting, for simplicity, the surface barrier edge currents, and assuming, for example, an exponential decay of $J_c(x)$ in Fig. 1b).

The a.c. response of the system should be distinctly different, because the contamination process occurs only near the edges, where the disordered lattice periodically penetrates and leaves the sample. For a square wave I_{ac} of period $T_{ac} = 1/f$, by the end of the positive half cycle the disordered phase occupies the left edge to a depth of x_d^{ac} , as illustrated by the solid curve in Fig. 1b. During the negative half cycle the disordered phase on the left leaves the sample, while a disordered phase on the right edge penetrates, until at $t = T_{ac}$ a mirror-image profile is obtained, as shown by the dashed line. Assuming $x_d^{ac} < W < L_r$, the effective I_c observed by a.c. transport measurement is given by $I_c^{ac} \approx dx_d^{ac} J_c^{dis} + d(W - x_d^{ac}) J_c^{ord}$. Thus, an alternating current necessarily contaminates the sample less than a direct current of the same amplitude, and therefore I_c^{ac} is always $\leq I_c^{dc}$, as seen in Fig. 1a. In addition, as x_d^{ac} decreases with frequency, I_c^{ac} should decrease with f , explaining the frequency dependence of I_c^{ac} in Fig. 1a. Furthermore, and most importantly,

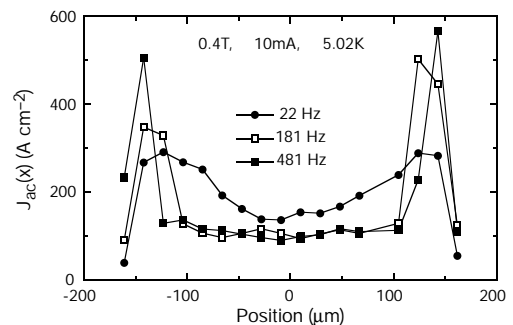


Figure 2 Current density profiles $J_{ac}(x)$ in crystal B. These are obtained by inversion of the self-induced field measured by the Hall sensors. Shown are results for three frequencies f , 22 Hz (filled circles), 181 Hz (open squares), and 481 Hz (filled squares). A square wave alternating current I_{ac} was applied, and the corresponding self-induced magnetic field $B_{ac}(x)$ across the crystal was measured by the Hall sensors using a lock-in amplifier (see Fig. 1 inset). By using the Biot-Savart law, $B_{ac}(x)$ was directly inverted²⁵ to give the current-density profiles $J_{ac}(x)$. The width x_d^{ac} of the highly pinned disordered phase near the edges grows with decreasing frequency, as expected. The measured $J_{ac}(x)$ is the magnitude of the local current density averaged over the a.c. cycle period. As a result, $J_{ac}(x)$ reflects a time-averaged superposition of solid and dashed $J_c(x, t)$ profiles in Fig. 1b, which are present separately during the positive and negative half-cycles. Close to the edges the high J is present most of the time, while close to x_d^{ac} it is present only a small fraction of the a.c. period as the disordered phase moves in and out of the sample. Therefore, the time-averaged $J_{ac}(x)$ decreases smoothly from the edge to x_d^{ac} . A more detailed analysis shows that the first-harmonic measurement by the lock-in amplifier Fourier-transforms the sharp instantaneous $J_c(x, t)$ of Fig. 1b into the observed smooth $J_{ac}(x) = J_c^{ord} + (J_c^{dis} - J_c^{ord})(1 + \cos(\pi x/x_d^{ac}))/2 + (J_c^{dis} - J_c^{ord})(1 - \cos(\pi(x + x_d^{ac} - W)/x_d^{ac}))/2$. The second and third terms hold at $0 \leq x \leq x_d^{ac}$ and $W - x_d^{ac} \leq x \leq W$, respectively, and are zero otherwise.

at sufficiently high frequency I_c^c should approach the true I_c of the stable phase. The steep increase of the 881-Hz I_{ac} data in Fig. 1a (open circles) therefore indicates that the ordered vortex phase transforms sharply into the disordered phase at the peak effect. In contrast, the smooth behaviour of I_c^d reflects rather the dynamic coexistence of the two phases, in which L_r gradually increases and diverges on approaching the peak effect from below. From Fig. 1a we can evaluate L_r and τ_r . For example, at $T = 5.1$ K, $I_c^c \approx 50$ mA is about half way between $I_c^{ord} \approx 5$ mA and the extrapolated $I_c^{dis} \approx 100$ mA, which means that $L_r \approx 0.5W = 170 \mu\text{m}$. The I_c^d was measured at a voltage criterion of $1 \mu\text{V}$, which translates into vortex velocity of $v \approx 4 \times 10^{-3} \text{ m s}^{-1}$, and hence $\tau_r = L_r/v \approx 4 \times 10^{-2} \text{ s}$. This value is well within the range of the relaxation times measured previously⁸ by applying a current step to the field-cooled metastable disordered vortex phase.

We now provide a direct experimental manifestation of the central aspect of the model, which is the spatial dependence of the disordered system and $J_c(x)$, and of the transport current distribution that traces this $J_c(x)$ (see Fig. 1b). We have used Hall sensor arrays to measure the a.c. transport current self-induced field^{25–27} $B_{ac}(x)$, which is then directly inverted to give the current density distribution $J_{ac}(x)$ using the Biot–Savart law, as described previously²⁵ (see Fig. 1a inset). Figure 2 shows the corresponding current density profiles $J_{ac}(x)$ measured at different frequencies. At high f , the disordered vortex phase with the enhanced J_c is present only in narrow regions near the edges (481-Hz data). As the frequency is reduced, x_d^{ac} grows and correspondingly the enhanced $J_{ac}(x)$ flows in wider regions near the edges. Note that our measurement procedure (see Fig. 2) provides the time-averaged local amplitude of $J_{ac}(x)$, which is much smoother than the sharp instantaneous profiles in Fig. 1b.

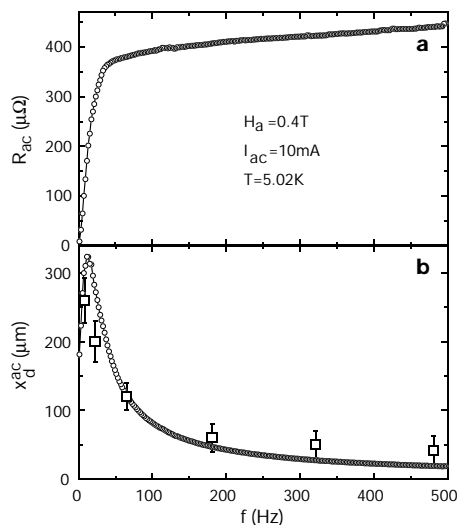


Figure 3 Frequency dependence of the resistance $R_{ac}(f)$ and of the width of the disordered regions x_d^{ac} in crystal B. **a**, At high frequencies R_{ac} is large, as most of the sample is in the weakly pinned ordered phase. As the frequency is decreased the disordered regions increase and R_{ac} drops sharply when x_d^{ac} reaches values close to the sample width. In the limit of zero f the resistance is zero as the applied current is lower than I_c^d . **b**, The corresponding width of the disordered phase near the edges x_d^{ac} derived from the $R_{ac}(f)$ data (circles) and from the $J_{ac}(x)$ current profiles of Fig. 2 (squares). As expected, x_d^{ac} increases monotonically with decreasing frequency. The decrease of the x_d^{ac} data (circles) at very low frequencies is an artefact. At such frequencies, the instantaneous vortex motion is present mainly at the onset of the square wave I_{dc} pulses, and decays towards zero during the pulse¹³. In this situation the first-harmonic R_{ac} measurement by the lock-in amplifier underestimates the integrated vortex displacement. In addition to the frequency dependence, x_d^{ac} also changes significantly when the amplitude of the a.c. current I_{ac} is varied. Here $I_{ac} = 10$ mA was chosen, such that x_d^{ac} becomes comparable to the sample width at low frequencies.

We confirm the above finding independently by measuring the corresponding a.c. resistance of the sample $R_{ac}(f)$ (Fig. 3a). At high frequencies, most of the sample is in the low pinning ordered phase and therefore R is large. As f is decreased, progressively wider regions near the edges become contaminated with the more strongly pinned disordered phase, and thus $R_{ac}(f)$ decreases. If the applied I_{ac} is larger than I_c^d , a finite R will be measured at all frequencies; but if $I_c^c \leq I_{ac} \leq I_c^d$ (see Fig. 1a), the measured R will vanish as $f \rightarrow 0$, as observed in Fig. 3a. This explains the surprising phenomenon of finite vortex response to a.c. current, while for d.c. drive the vortex motion is absent^{13,15,16}. One can directly calculate the width of the disordered regions from $R_{ac}(f)$ by noting that x_d^{ac} equals the distance the entire lattice is displaced during half an a.c. period; $x_d^{ac}(f) = v/2f = R(f)I_{ac}/2fLB$, where L is the voltage contact separation. The open circles in Fig. 3b show x_d^{ac} obtained from $R_{ac}(f)$, while the open squares show the x_d^{ac} derived directly from the $J_{ac}(x)$ profiles of Fig. 2. The good correspondence between the two independent evaluations of x_d^{ac} demonstrates the self-consistency of the model.

Next we address the extreme sensitivity of the a.c. response to a small d.c. bias¹³, as shown in Fig. 4a, where R_{ac} is presented as a function of a superposed I_{dc} . A d.c. bias of only 10% to 20% of I_{ac} suppresses R_{ac} by orders of magnitude. This behaviour is a natural consequence of the described mechanism, because the d.c. bias contaminates the sample very similarly to the pure d.c. case, except that L_r is now renormalized as follows. For $I_{dc} \ll I_{ac}$, the vortices move back and forth during the a.c. cycle, with a forward displacement being larger by about $2I_{dc}/I_{ac}$. Therefore, a vortex that enters through the sample edge and reaches a position accumulates a much longer total displacement path of xI_{dc}/I_{ac} . Because the annealing process of the disordered vortex phase depends on the total

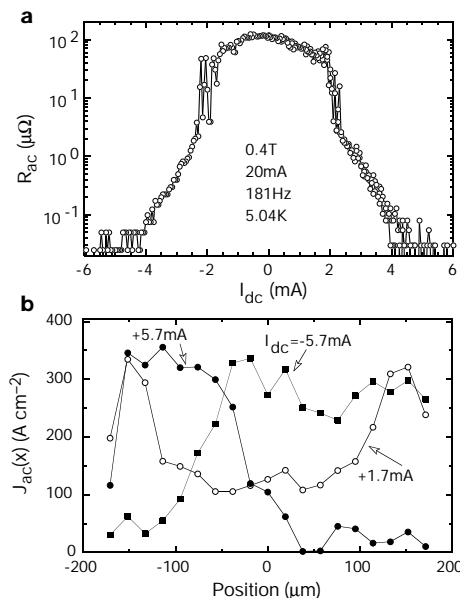


Figure 4 Measured resistance as a function of d.c. bias, and the corresponding distribution of the alternating current in crystal A. **a**, At low d.c. bias, $I_{dc} \leq 2$ mA, only the regions near the edges are contaminated by the disordered vortex phase as L_r^{eff} is very short, resulting in only a moderate decrease of the measured resistance R_{ac} . ($I_{ac} = 20$ mA for all R_{ac} measurements shown here.) For $I_{dc} \geq 2$ mA, the contamination becomes substantial, and the significant decrease of R_{ac} is accompanied by enhanced noise due to the local instabilities during the competing contamination and annealing processes. At still larger d.c. bias, most of the sample becomes contaminated and R_{ac} drops below our noise level. The corresponding $J_{ac}(x)$ profiles in **b** show that for positive $I_{dc} = +5.7$ mA (filled circles) a substantial part of the sample is contaminated from the left edge where the vortices enter the crystal, and similarly from the right edge for negative bias $I_{dc} = -5.7$ mA (filled squares).

displacement regardless of the direction, the lattice at this location is thus annealed substantially, as if the effective L_r is reduced to $L_r^{\text{eff}} \approx L_r I_{dc} / I_{ac}$. Thus, at very small biases, the disordered phase is present only within x_d^{ad} from the edges, as in the absence of a bias, where the disordered vortices leave and re-penetrate every cycle. Vortices that drift deeper into the bulk under the influence of I_{dc} are practically fully annealed because of the very short L_r^{eff} . As a result, the initial decrease of R_{ac} up to $I_{dc} \approx 2$ mA (see Fig. 4a) is relatively small. The corresponding $J_{ac}(x)$ in Fig. 4b at $I_{dc} = 1.7$ mA shows narrow contaminated regions near the edges, very similar to the zero-bias case in Fig. 2. However, as I_{dc} is increased, L_r^{eff} grows and the bulk of the sample becomes contaminated by the penetrating disordered vortex phase, leading to a marked drop of R_{ac} . In this situation, $J_{ac}(x)$ at $I_{dc} = 5.7$ mA shows a wide region of disordered phase at the left edge. When I_{dc} is inverted to -5.7 mA, a similar situation is observed, but now the vortices—and hence the disordered phase—penetrate from the right edge, as expected.

The revealed mechanism readily explains a wide range of additional reported phenomena. (1) The history of the previously applied current is encoded in the spatial profile of the lattice disorder, which is preserved after the current is switched off owing to negligible thermal relaxation. On reapplying the current, the vortex system will display a memory of all the parameters of the previously applied current, including its direction, duration, amplitude and frequency, as observed experimentally^{13,14}. (2) Application of a current step $I < I_{dc}^{\text{dc}}$ to a sample in the ordered vortex phase results in a transient response which decays to zero, as the disordered phase is able to penetrate only a limited distance. The resulting new I_c of the sample is given by the condition that $I_c = I$, as derived by fast transport measurements^{14,15}. Such transient phenomena would also display characteristic times shorter than, or comparable to, the vortex transit time across the sample, in agreement with observations^{13,14}. (3) The competition between the contamination and annealing processes is expected to result in local instabilities, causing the reported noise enhancement below the peak effect^{1,2} (see also Fig. 4a). (4) Related phenomena should be observed in high-temperature superconductors in the vicinity of the peak effect associated with the melting transition, or near the second magnetization peak, consistent with experiments^{3–6,12,16}. (5) In high-temperature superconductors there is an additional consideration of thermal activation of vortices over the surface barriers, which may explain the reported slow voltage oscillations^{3–6}. If the thermal activation rate is higher than, or comparable to, the driving rate, the slowly injected lattice will be ordered, in contrast to the disordered vortex phase injected at higher drives. Thus, at a given applied current, if the bulk of the sample is in the ordered vortex phase, much of the current flows on the edges, rapidly injecting a disordered vortex phase through the surface barrier. Once the bulk becomes contaminated, the resulting slower vortex motion again causes injection of an ordered phase. This feedback mechanism can explain the voltage oscillations^{3,6} in $\text{YBa}_2\text{Cu}_3\text{O}_7$ and similar narrow-band noise^{4,5} in $\text{YBa}_2\text{Cu}_3\text{O}_7$ and $\text{Bi}_2\text{Sr}_2\text{CaCu}_2\text{O}_8$ with characteristic frequencies comparable to the inverse transit time. Last, we note that the described phenomena should be absent in the Corbino disk geometry where vortices do not cross the sample edges. Our studies of NbSe_2 in this geometry (Y.P. *et al.*, manuscript in preparation) confirm this prediction. □

Received 5 August; accepted 16 November 1999.

1. Marley, A. C., Higgins, M. J. & Bhattacharya, S. Flux flow noise and dynamical transitions in a flux line lattice. *Phys. Rev. Lett.* **74**, 3029–3032 (1995).
2. Merithew, R. D. *et al.* Persistent metastable states in vortex flow at the peak effect in NbSe_2 . *Phys. Rev. Lett.* **77**, 3197–3199 (1996).
3. Kwok, W. K. *et al.* Dynamic instabilities in the vortex lattice of $\text{YBa}_2\text{Cu}_3\text{O}_7$. *Physica C* **293**, 111–117 (1997).
4. D'Anna, G. *et al.* Vortex-motion-induced voltage noise in $\text{YBa}_2\text{Cu}_3\text{O}_7$ single crystals. *Phys. Rev. Lett.* **75**, 3521–3524 (1995).
5. Tsuboi, T., Hanaguri, T. & Maeda, A. Local density fluctuations of moving vortices in the solid and liquid phases in $\text{Bi}_2\text{Sr}_2\text{CaCu}_2\text{O}_8$. *Phys. Rev. Lett.* **80**, 4550–4553 (1998).

6. Gordeev, S. N. *et al.* Current-induced organization of vortex motion in type-II superconductors. *Nature* **385**, 324–326 (1997).
7. Bhattacharya, S. & Higgins, M. J. Flux-flow fingerprint of disorder: melting versus tearing of a flux-line lattice. *Phys. Rev. B* **52**, 64–67 (1995).
8. Henderson, W. *et al.* Metastability and glassy behavior of a driven flux-line lattice. *Phys. Rev. Lett.* **77**, 2077–2080 (1996).
9. Banerjee, S. S. *et al.* Anomalous peak effect in CeRu_2 and 2H-NbSe_2 : Fracturing of a flux line lattice. *Phys. Rev. B* **58**, 995–999 (1999).
10. Banerjee, S. S. *et al.* Metastability and switching in the vortex state of 2H-NbSe_2 . *Appl. Phys. Lett.* **74**, 126–128 (1999).
11. Wordenweber, R., Kes, P. H. & Tsuei, C. C. Peak and history effect in two-dimensional collective flux pinning. *Phys. Rev. B* **33**, 3172–3180 (1986).
12. Kokkalis, S. *et al.* Onset of plasticity and hardening of the hysteretic response in the vortex system of $\text{YBa}_2\text{Cu}_3\text{O}_{7-\delta}$. *Phys. Rev. Lett.* **82**, 5116–5119 (1999).
13. Henderson, W., Andrei, E. Y. & Higgins, M. J. Plastic motion of a vortex lattice driven by alternating current. *Phys. Rev. Lett.* **81**, 2352–2355 (1998).
14. Xiao, Z. L., Andrei, E. Y. & Higgins, M. J. Flow induced organization and memory of a vortex lattice. *Phys. Rev. Lett.* **83**, 1664–1667 (1999).
15. Andrei, E. Y. *et al.* Current driven organization of magnetic vortices. *J. Phys. IV* **10**, 5–10 (1999).
16. Metlushko, V. *et al.* Driven vortex states and relaxation in single crystal $\text{YBa}_2\text{Cu}_3\text{O}_8$. Preprint cond-mat/9804121 at (<http://xxx.lanl.gov>) (1999).
17. Gammel, P. L. *et al.* Structure and correlation of a flux line lattice in crystalline Nb through peak effect. *Phys. Rev. Lett.* **80**, 833–836 (1998).
18. Khaykovich, B. *et al.* Vortex-lattice phase transitions in $\text{Bi}_2\text{Sr}_2\text{CaCu}_2\text{O}_8$ crystals with different oxygen stoichiometry. *Phys. Rev. Lett.* **76**, 2555–2558 (1996).
19. Giamarchi, T. & Le Doussal, P. Elastic theory of pinned flux lattices. *Phys. Rev. Lett.* **72**, 1530–1533 (1994).
20. Ertas, D. & Nelson, D. R. Irreversibility, mechanical entanglement and thermal melting in superconducting vortex crystal with point impurities. *Physica C* **272**, 79–85 (1996).
21. Vinokur, V. *et al.* Lindemann criterion and vortex-matter phase transitions in high-temperature superconductors. *Physica C* **295**, 209–217 (1998).
22. Pardo, F. *et al.* Topological defects in the flux-line lattice and their relationship to the critical current of a type-II superconductor. *Phys. Rev. Lett.* **78**, 4633–4636 (1996).
23. Yaron, U. *et al.* Structural evidence for a two-step process in the depinning of the superconducting flux-line lattice. *Nature* **376**, 753–755 (1995).
24. Bean, C. P. & Livingston, J. D. Surface barrier in type-II superconductors. *Phys. Rev. Lett.* **12**, 14–16 (1964).
25. Paltiel, Y. *et al.* Surface barrier dominated transport in NbSe_2 . *Phys. Rev. B* **58**, R14763–R14766 (1998).
26. Fuchs, D. T. *et al.* Transport properties governed by surface barriers in $\text{Bi}_2\text{Sr}_2\text{CaCu}_2\text{O}_8$. *Nature* **391**, 373–376 (1998).
27. Fuchs, D. T. *et al.* Possible new vortex matter phases in $\text{Bi}_2\text{Sr}_2\text{CaCu}_2\text{O}_8$. *Phys. Rev. Lett.* **80**, 4971–4974 (1998).
28. Burlachkov, L., Koshelev, A. E. & Vinokur, V. M. Transport properties of high-temperature superconductors: surface vs. bulk effect. *Phys. Rev. B* **54**, 6750–6757 (1996).

Acknowledgements

We thank P. B. Littlewood for discussions. The work at the Weizmann Institute of Science was supported by the Israel Science Foundation—Centre of Excellence Program, by the US–Israel Binational Science Foundation (BSF), and by the Alhadeff research award. E.Y.A. was supported by the NSF.

Correspondence and requests for materials should be addressed to Y.P. (e-mail: hpalt@wis.weizmann.ac.il).

Singularity dynamics in curvature collapse and jet eruption on a fluid surface

Benjamin W. Zeff*, Benjamin Kleber*, Jay Fineberg† & Daniel P. Lathrop*

* Institute for Plasma Research and Department of Physics, The University of Maryland, College Park, Maryland 20742, USA

† The Racah Institute of Physics, The Hebrew University of Jerusalem, Jerusalem, Israel

Finite-time singularities—local divergences in the amplitude or gradient of a physical observable at a particular time—occur in a diverse range of physical systems. Examples include singularities capable of damaging optical fibres and lasers in nonlinear optical systems¹, and gravitational singularities² associated with black holes. In fluid systems, the formation of finite-time singularities